Interference and stabilization in the quasibound Stark spectrum

C. Chardonnet,* D. Delande, and J. C. Gay
Laboratoire de Spectroscopie Hertzienne de l'Ecole Normale Supérieure, Université Paris 6, T12-E01, 4 place Jussieu 75252 Paris CEDEX 05, France
(Received 28 March 1988; revised manuscript received 29 June 1988)

Experimental studies of the quasibound Stark spectrum of cesium are reported with emphasis on the Stark redistribution of nonhydrogenic states onto the linear Stark manifold. We show that most characteristics of the spectra are understood with analytical models describing the interaction of one or several discrete states with one or several quasicontinua of discrete states. In particular, we give experimental evidence for the discrete versions of Fano profiles and stabilization of states due to interference effects. These are also important features of the continuum region which several experiments have recently demonstrated.

I. INTRODUCTION

In this paper we present and discuss experimental results that concern the Stark redistribution of nonhydrogenic states onto the manifold of states which are linearly Stark quantized. Previous studies in the continuum region have shown that the breaking of the Stark dynamical symmetry in nonhydrogenic atoms leads to several features, such as the generation of Fano profiles and stabilization processes (also called "interference narrowing") arising from interference effects[1–9] between the Stark channels. Fairly good interpretation is obtained by the means of Harmin's theory[4–6] and numerical calculations.[7]

Similar phenomena affect the quasibound part of the Stark spectra below the classical ionization limit. Fano profiles spread over discrete series and stabilization effects arising from interfering discrete channels are experimentally recorded. Here, a completely analytical description is possible and successful by extending the earlier model by Fano[8] (in 1935) describing the interaction of one discrete state with a set of discrete states acting as a quasicontinuum. The use of the general theoretical approach recently developed by Harmin[6] and Liu *et al.*[9] in the case of interference narrowing is here not necessary, though it is a necessary step in interpreting the data in the true continua regions. Previous limited reports of the present work have been described in Refs. 10–12. Both experimental and theoretical approaches complement each other quite nicely and afford an important clarification of the physics of the Stark effect and its role in line-shape formation.

Section II is devoted to a basic review of the Stark effect on nonhydrogenic species. Section III recalls and extends the theory of one discrete state interacting with a quasicontinuum of discrete states. Section IV focusses on experimental results, generation of pseudo-Fano profiles and decoupling of states from the quasicontinua. An analytic interpretation of the results is given in Sec. V and compared with a numerical theory.

Notations are E for the energy and $\mathbf{F}$ for the electric field. Atomic units are used and for the electric field are associated with the value $F_c = 5.14 \times 10^9$ V/cm.

II. STARK EFFECT ON NONHYDROGENIC SPECIES—REVIEW

A. The Stark effect: General considerations

The interaction of an electric field with hydrogenic species has attracted much attention for years. For the hydrogen atom, the existence of a dynamical symmetry makes the problem tractable in a formal way. Writing the Hamiltonian (in atomic units),

$$H = \frac{p^2}{2} - \frac{1}{r} + \mathbf{F}\cdot\mathbf{r} , \tag{1}$$

the projection of the angular momentum $\mathbf{L} = \mathbf{r} \times \mathbf{p}$ on the $\mathbf{F}$ field axis is a constant of motion. Another one is $\tilde{A}_z$, the dynamical constant deduced from the Runge-Lenz vector.[13] The set of commuting observables $(H, L_z, \tilde{A}_z)$ allows for a complete classification of the spectrum and eigenfunctions.

The standard treatment based on the separability of the Schrödinger equation in parabolic coordinates (ξ, η, φ) allows one to show that the ξ motion is bounded while the η motion is shaped by the barrier and may be unbounded.[7] The resonance character of the states is thus enhanced close to the maximum of the barrier. This is associated roughly with the so-called classical ionization energy $E_c = -2\sqrt{F}$. For $E < E_c$, the spectrum is quasibound, labeled with the eigenvalue of $A_z = (n_2 - n_1)/n$ where (n_1, n_2) are the parabolic quantum numbers. A consequence of the dynamical symmetry and separability is that the states associated with different values of the parabolic quantum numbers do cross. Consequently, the states can be labeled through these zero-field quantum numbers, up to the classical ionization field.

B. Stark effect in nonhydrogenic species

When the effective potential acting upon the electron is not Coulombic, the Stark dynamical symmetry is destroyed. But at sufficiently large r, the hydrogenic behavior should be recovered asymptotically as the potential is nearly Coulombic while at small r, non-Coulombic corrections are dominant over the Stark interaction.

Hence the solution to the Stark problem for nonhydrogenic atoms is mainly one of the connection between these two regions of spherical and parabolic symmetries. This has been solved quite generally by Harmin[4–6] and applies successfully to most experimental situations[9] as well as to similar problems.[14]

Experimental consequences of this breaking of the symmetries lie in the general noncrossing rule of the energy levels. Optical excitation of the interacting Stark channels leads to the generation of Fano profiles under varied conditions[2,3] and to the stabilization of resonances[9,15,16] embedded in the continua, through destructive interference effects.

C. Unified treatment of the quasibound Stark spectra

The quasibound Stark spectrum at low fields is the domain of the linear Stark effect. The Coulomb symmetry is reorganized along the subgroup chain $SO(4)\supset SO(2)\otimes SO(2)$ of the parabolic type. In contrast with the high-field limit, most of the physics can be analyzed in detail with elementary calculations. This is especially true for the question of nonhydrogenic effects.[10]

The energy-level structure of the hydrogen atom is[17]

$$E=-\frac{1}{2n^2}+\tfrac{3}{2}nFq+O(F^2)+\cdots\ ,$$
$$q=n_1-n_2;n=n_1+n_2+|m|+1\ ; \tag{2}$$

q is the difference of the zero-field parabolic quantum numbers. The odd or even character of $|m|-q$ is fixed by the n value. The spectrum depends only on $|m|$.

At fixed m, the linear Stark spectrum is composed of a set of $n-|m|$ sublevels (labeled with q), the spacing of which is $2\omega_s$, where $\omega_s=\frac{3}{2}nF$ a.u. is the linear Stark frequency. The spectrum of two manifolds for m and $m+1$ are shifted by ω_s from each other [see, e.g., Fig. 1(a)]. Finally, the degeneracy on the m value of each q sublevel is $n-|q|$. The eigenfunctions are the zero-field parabolic ones.

The extension of a Stark manifold being $2n\omega_s$ (for $|M|\ll n$) and the spacing between two manifolds $1/n^3$, then a condition for merging of the Stark manifolds is $n^4\omega_s\simeq\frac{1}{2}$ or $n^5F\simeq\frac{1}{3}$. In hydrogen, the energy levels cross without interaction.[18,19]

When the effective potential acting upon the electron is not Coulombic, the n^2 degeneracy of the n shell is removed. In high Rydberg states of alkali-metal atoms, there are, however, clues that the system will behave hydrogenically. Actually the wave functions of most states are concentrated in regions where the departures from a Coulomb field are small, leading to small quantum defects. Penetrating states (usually for $l\leq 2$) are an exception leading to nondegeneracy of the l value. We call these states (S, P, and D) "nonhydrogenic states." For $l\geq 3$, quantum defects are negligibly small and these (n^2-9) states build an incomplete hydrogenic manifold.[10] Owing to their degeneracy, they should exhibit a linear Stark behavior in the field, in contrast to the nonhydrogenic ones. Further interaction between the two classes of states described hereafter as "Stark redistribution of nonhydrogenic states" is the matter of this paper.[11,12,20]

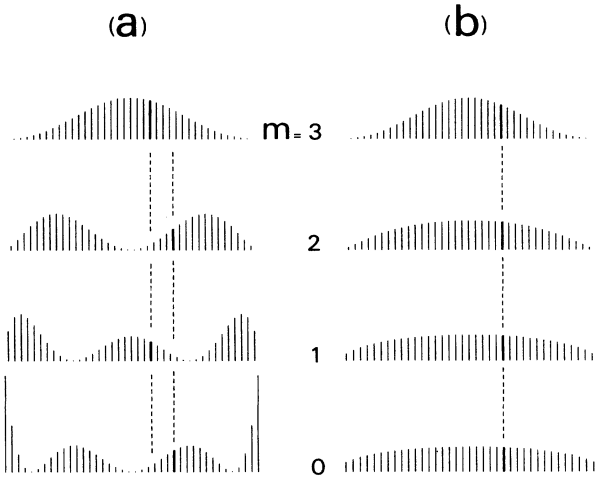

FIG. 1. Comparison of the spectrum and oscillator strengths distribution for the complete (a) and incomplete (b) Stark manifolds. Removing one level shifts the spectrum by ω_s. However, as the spectra of the complete manifolds are also shifted by ω_s according to m being odd or even, this makes the incomplete $m=0,1,2$ manifold spectra very similar to the spectra of a complete $m=3$ manifold. In addition, the distribution of the F state becomes similar.

D. The incomplete manifold treatment

The properties of an incomplete manifold at low field are very easy to deduce in a standard way. The essential difference with the situation in hydrogen is that states with $l\leq 2$ are out of this manifold. Both the spectrum and eigenfunctions are thus deduced from the complete SO(4) situation using a resolvent formalism (see, for example, Refs. 10 and 20–22).

The conclusions are summarized in Fig. 1, where the spectrum and oscillator strengths distributions (of the F state) of both the complete and incomplete ($m=0,1,2,3$) manifolds are compared. Although the distributions are very different when the manifolds are complete, they become fairly similar to those of the $m=3$ complete case when the $m=0,1,2$ manifolds are incomplete. The number of components is $n-3$. The Stark effect is still linear and the spacing is approximately[11] $2\omega_s$, but the energies of the sublevels are shifted by ω_s when one level is removed (Fig. 1 and Sec. III).[10] When the electric field is increased, the nonhydrogenic states (experiencing a quadratic Stark effect) should interact with the incomplete manifold of states spaced with $2\omega_s$, which can be modeled as a quasicontinuum of discrete states.

The Stark redistribution of nonhydrogenic states can be described in the framework of a very simple analytical model of "one discrete state interacting with a quasicontinuum of discrete states."

III. GENERAL FRAMEWORK—ONE DISCRETE STATE INTERACTING WITH A QUASICONTINUUM OF DISCRETE STATES

Such a situation has been considered by Fano[8,23] over 50 years ago and finds here one of its most striking experimental realization.

A. Simple model of the perturbed spectrum

The model involves one discrete state $|\varphi\rangle$ interacting with a set of N discrete states $\{|\psi_p\rangle; 1\le p\le N\}$. These are eigenstates of the Hamiltonian H_0 with energies E_φ and E_p, respectively. This is schematized in Fig. 2(a).

When the coupling V between $|\varphi\rangle$ *and* the manifold is included, the eigenstates of $H=H_0+V$ become $\{|\chi_q\rangle; 1\le q\le N+1\}$ such that $H|\chi_q\rangle=E'_q|\chi_q\rangle$. Their explicit form is

$$|\chi_q\rangle=a_q|\varphi\rangle+\sum_{p=1}^{N} b_{qp}|\psi_p\rangle\ ,$$
$$b_{qp}=a_q V_p(E'_q-E_p)^{-1}\ , \tag{3}$$

$$a_q=\left[1+\sum_{p=1}^{N}\frac{|V_p|^2}{(E'_q-E_p)^2}\right]^{-1/2}\ , \tag{4}$$

where we have defined[8] $V_p=\langle\psi_p|V|\varphi\rangle$. The perturbed energy spectrum $\{E'_q; 1\le q\le N+1\}$ (obviously differing from $\{E_p\}$) is given by the implicit equation

$$f(E'_q)=E'_q-E_\varphi=\sum_{p=1}^{N}\frac{|V_p|^2}{E'_q-E_p} \tag{5}$$

and a_q is rewritten as

$$a_q=\left[1-\frac{df(E'_q)}{dE'_q}\right]^{-1/2}\ . \tag{6}$$

A graphical representation of Eq. (5) is shown in Fig. 3. The poles of $f(E)$ are the unperturbed energies $\{E_p\}$ with weight $|V_p|^2$. The new eigenspectrum is given by the intersection with the straight line (E'_q-E_φ). The distribution a_q of the discrete state onto the new eigenstates essentially depends on the slope of $f(E)$ at E'_q.

These equations can be cast in closed form in various special cases. For an infinite manifold of equally spaced sublevels (with spacing ω), the poles $\{E_p=p\omega\}$ coincide with those of the $\cot(\pi E/\omega)$ function. When the coupling is constant over the (infinite) manifold ($|V_p|=|V|$), the summation in Eq. (5) can be performed exactly[24] as

$$E'_q-E_\varphi=\sum_{p=1}^{\infty}\frac{|V_p|^2}{E'_q-E_p}=\frac{\pi}{\omega}|V|^2\cot\left[\frac{\pi E'_q}{\omega}\right]\ .$$

When the coupling is slowly varying with p, the procedure can be amended by expanding the coupling at the energy E'_q as $|V_p|^2=(|V_p|^2-|V_q|^2)+|V_q|^2$. Here $|V_q|^2$ stands for the local value of the coupling at the unperturbed state numbered q (whose energy E_q is just above E'_q).[25] Hence, Eqs. (4) and (5) give

$$\frac{\pi}{\omega}|V_q|^2\cot\left[\frac{\pi E'_q}{\omega}\right]\simeq E'_q-E_\varphi-F_q \tag{7}$$

and

$$a_q=\left[1+G_q+\frac{\pi^2|V_q|^2}{\omega^2}+\frac{(E'_q-E_\varphi-F_q)^2}{|V_q|^2}\right]^{-1/2} \tag{8}$$

where F_q and G_q are

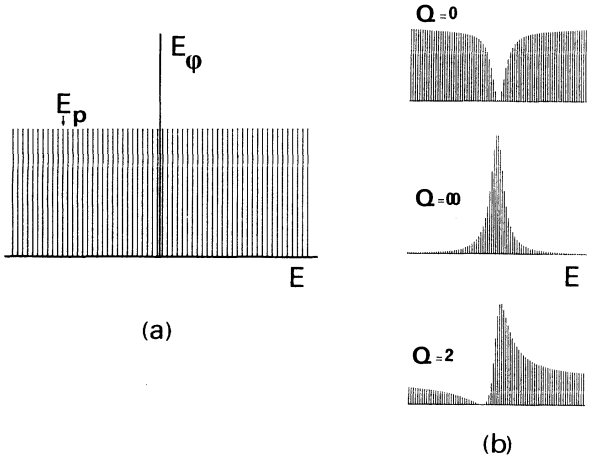

FIG. 2. One discrete state interacting with a quasicontinuum of discrete states. (a) Without interaction between the discrete state $|\varphi\rangle$ (with energy E_φ) and the manifold $\{|\psi_p\rangle; 1\le p\le N\}$ (with energy E_p). (b) Interaction taken into account. This may lead to the generation of Fano-shaped profiles in the intensity distribution of the discrete lines, shown for three values of the Fano parameter Q.

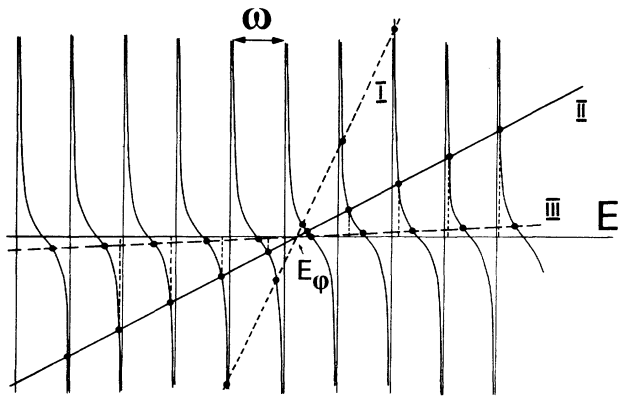

FIG. 3. Graphical solution of the eigenvalue equations (case of an equally-spaced infinite manifold). The unperturbed energies E_p are poles of $f(E)$. The resulting spectrum is obtained through the intersection of $f(E)$ with a straight line $(\omega/\pi|V|^2)(E-E_\varphi)$ in the case of constant coupling. According to the slope $\omega/\pi|V|^2$ one obtains the anticrossing regime (I), the Fano-type situation (several levels around E_φ are affected) (II), and strong redistribution (III) in which all the energies are shifted by $\omega/2$.

$$F_q = F(E'_q) = \sum_p \frac{|V_p|^2 - |V_q|^2}{E'_q - E_p} , \tag{9}$$

$$G_q = G(E'_q) = \sum_p \frac{|V_p|^2 - |V_q|^2}{(E'_q - E_p)^2} . \tag{10}$$

F_q and G_q express, respectively, a shift and broadening of the distribution of the discrete state onto the manifold due to the variations of the coupling. The shift vanishes when the situation is symmetrical both as concerns the positions and distributions of $|V_p|^2$.

B. Physical implications of the model

From Eq. (8), the distribution $|a_q|^2$ of the discrete state onto the manifold is Lorentzian shaped, with a width

$$\Gamma = 2\pi \frac{|V_q|^2}{\omega} \left[1 + \frac{\omega^2}{\pi^2 |V_q|^2} \right]^{1/2} , \tag{11}$$

where the negligibly small G_q correction to the broadening has been dropped. The variations of F_q and G_q with the quasicontinuous energy parameter E'_q may generate small asymmetries.[24] From Eq. (11) and Fig. 3, there are three principal regimes in the redistribution of the discrete state $|\varphi\rangle$ onto the manifold.

(1) The anticrossing regime when $|V| \ll \omega$ (case I in Fig. 3). The perturbation is local leading to anticrossings with one state of the manifold. The width of $|a_q|^2$ is $\Gamma \sim 2|V| \ll \omega$ and the slope $\omega/\pi|V_q|^2$ [Eq. (7)] is nearly infinite. Most of the spectrum is unperturbed.

(2) The redistribution regime when $|V| \gtrsim \omega$ (case II in Fig. 3). The discrete state is redistributed onto $\Gamma/\omega \simeq 2\pi|V|^2/\omega^2$ states of the manifold, the energies of which are perturbed.

(3) The strong-coupling regime when $|V| \gg \omega$ (case III in Fig. 3). The discrete state is redistributed onto most of the states of the manifold. When $|V|/\omega \to \infty$ the redistribution is complete and from Fig. 3 the new eigenenergies are shifted by $\omega/2$ compared with the unperturbed ones. This character (see Sec. II D) has already been found when comparing a complete and incomplete manifold spectrum (Fig. 1).

C. Optical excitation and pseudo-Fano profiles

The appearance of the redistribution process is likely to be strongly affected by interference effects when optical excitation of both the discrete state $|\varphi\rangle$ and of the manifold is possible. Denoting T as the transition operator, we define $T_\varphi = \langle \varphi | T | i \rangle$, $T_p = \langle \psi_p | T | i \rangle$ where $|i\rangle$ is the lower level of the transition. Then the amplitude of excitation of $|\chi_q\rangle$ is

$$\langle \chi_q | T | i \rangle = a_q \left[T_\varphi + \sum_p \frac{V_p T_p}{E'_q - E_p} \right] . \tag{12}$$

The second term arises from the combined effects of excitation and coupling, and can be simplified through elementary manipulations and use of Eq. (5). The probability of transition at energy E'_q (normalized to $|T_q|^2$) is

$$I = \frac{|\langle \chi_q | T | i \rangle|^2}{|\langle \psi_q | T | i \rangle|^2} = \frac{(Q + \varepsilon_q)^2}{1 + \varepsilon_q^2} , \tag{13}$$

with

$$\varepsilon_q = (E'_q - E_\varphi - F_q)/(\Gamma/2) , \tag{14}$$

$$Q = \frac{2V_q}{\Gamma T_q}(T_\varphi + H_q) , \tag{15}$$

where

$$H_q = \sum_{p=1}^{N} \frac{V_p T_p - V_q T_q}{E'_q - E_p} . \tag{16}$$

When the spacing ω between two adjacent states is smaller than the width Γ, then the eigenenergies $\{E'_q\}$ constitute a quasicontinuous energy variable. Hence, provided that Γ, F_q, and Q are smooth functions of the energy, Eq. (13) describes a quasicontinuous Fano profile with parameter Q.[25] The excitation profile is thus asymmetric. As shown in Fig. 2, I is the envelope of the set of discrete lines. As in the continuous case, interference effects make the distribution very different from the quasi-Lorentzian shaped $|a_q|^2$. The maximum of I is associated with $\varepsilon_q = 1/Q$ and the minimum with $\varepsilon_q = -Q$. Even if the excitation probability T_φ of the discrete state is zero, the profile is still asymmetric if $H_q \neq 0$. H_q is analogous to a shift arising from mixed effects of the variations of the transition probability and coupling over the manifold. A case of special interest (see Sec. V) is when the matrix elements T_p and V_p are proportional. This is the situation when optical excitation of the manifold states and coupling to the discrete state $|\varphi\rangle$ are through the same state of the manifold. From (16), H_q is then proportional to the shift F_q of the discrete state. Equation (15) thus becomes

$$Q = \frac{2}{\Gamma}(F_q + \Delta) , \qquad \Delta = \frac{V_q}{T_q} T_\varphi . \tag{17}$$

Finally, the previous analysis extends to the case of a discrete state interacting with a continuum by considering the eigenfunctions $|\psi_p\rangle/\omega^{1/2}$ normalized per unit energy, when $\omega \to 0$. The anticrossing regime (Sec. III B) no longer exists and interference profiles become established once the interaction V is nonzero. The results agree with the analysis of Fano.[23]

D. Stabilization effects for two discrete states interacting with a quasicontinuum

When two discrete states $|\varphi_1\rangle$ and $|\varphi_2\rangle$ interact with a quasicontinuum and with each other, the process may lead to complete decoupling of one state from the quasicontinuum through interference effects.

Such a situation is realized for the $m=1$ Stark spectrum of Cesium to be discussed in Sec. V C (see Fig. 4). The interaction V (the Stark Hamiltonian) depends on the parameter F (the electric field strength) as $V = F\mathcal{V}$.

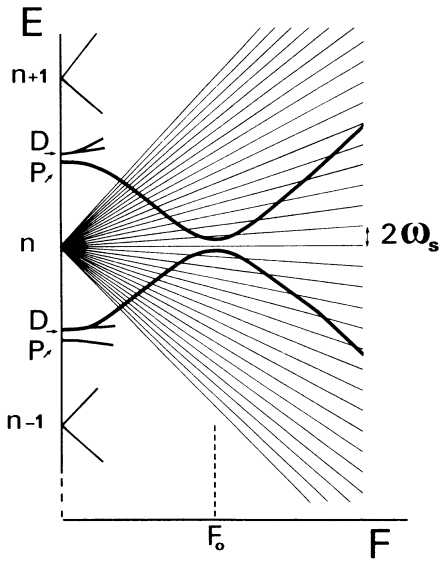

FIG. 4. Schematic representation of the situation of two discrete states interacting with a quasicontinuum of discrete states. This refers to the situation in cesium for the $m=1$ states. Interference effects at anticrossings lead to the decoupling of one state (stabilization) from the other channels.

Thus, $\mathcal{V}$ is the dipole moment operator. We assume here that $|\varphi_1\rangle$ and $|\varphi_2\rangle$ interact with the manifold through some $|\varphi_0\rangle$ component such that $\langle\varphi_i|\mathcal{V}|\varphi_0\rangle=\mathcal{V}_i$ and with each other with $\langle\varphi_i|\mathcal{V}|\varphi_j\rangle=\mathcal{V}_{ij}$. These transition matrix elements differ from the hydrogenic ones due to the quantum defects in cesium.

The interaction of the two discrete states leads to an anticrossing of their energy curves. The passing through anticrossing results in the transformation $|\varphi_1\rangle\rightarrow-|\varphi_2\rangle$ and $|\varphi_2\rangle\rightarrow|\varphi_1\rangle$ of the eigenfunctions $|\chi_{1,2}\rangle$. Their couplings with the manifold $\langle\chi_{1,2}|\mathcal{V}|\varphi_0\rangle$ thus evolve as $\mathcal{V}_1\rightarrow-\mathcal{V}_2$ and $\mathcal{V}_2\rightarrow\mathcal{V}_1$. Hence one of the two states has zero coupling with the manifold at some field value F_d. Denoting F_0 the field value at the anticrossing, one can obtain

$$F_d=\frac{F_0}{1+\mathcal{V}_{12}(\mathcal{V}_2^2-\mathcal{V}_1^2)/\mathcal{V}_1\mathcal{V}_2(\mathcal{V}_{11}-\mathcal{V}_{22})} \tag{18}$$

and

$$|\Phi\rangle_d\propto(\mathcal{V}_1|\varphi_2\rangle-\mathcal{V}_2|\varphi_1\rangle)\ .$$

Hence, two discrete states interacting with a manifold lead to pseudoprofiles as described in Sec. III C, but further interaction of these two profiles results in a decoupling of one state through interference at a given field value. A discrete state is thus stabilized with no interaction in the otherwise interacting channels, at a specific nonzero field value. This process is obviously analogous to the creation of quasibound states embedded in the continua.[26]

IV. EXPERIMENT

We describe here the experimental conditions for the observation of the previous effects in the Stark redistribution of nonhydrogenic states of cesium. Detailed analysis of the results will be given in Sec. V.

A. Experimental setup

Cw dye laser excitation of the nF and nP cesium Rydberg series is achieved from the ground state $|6S_{1/2}\rangle$ using the "hybrid resonance" process.[27] This amounts to populating the $|5D_{5/2,3/2}\rangle$ states through nonresonant absorption of one photon, followed by resonant absorption of one more photon, allowing efficient excitation of the $|nF\rangle$ and $|nP\rangle$ Rydberg series (up to $n\simeq160$). The process is Doppler limited. Detection of the Rydberg series is performed by the means of a thermoionic detector with an amplification factor of the order of 10^3.

The cw-ring dye laser, Ar^+ pumped, is servocontrolled to 1 MHz and allows a 150-GHz frequency scan by locking it to an external cavity which is presure swept, or 250-GHz electronic scans. The laser frequency can be modulated by typically 200 MHz at a modulation frequency around 95 Hz. Either amplitude modulation (AM) with a chopper or frequency modulation (FM) have been used, followed by convenient phase sensitive detection.

The cell contains the electrode arrangements for applying the electric field in the interaction region, between a plate and a mesh. The field homogeneity is better than 0.02 V/cm. The detection region which is electrostatically shielded from the other one contains a 800-K heated tungsten wire, 0.15 mm in diameter, which develops an electronic space charge. Stray electric fields are no more than 0.05 V/cm.

The pressure is kept low enough ($\simeq10^{-2}$ Torr) to avoid molecular background and collisional perturbations of the signal. The range of applied fields (supplied with a battery) is limited to 0–20 V/cm. Higher values trigger the lighting of discharges.

B. Excitation scheme in electric field

According to the laser polarization, the excitation can be changed from hydrogenic to nonhydrogenic in the same atom. There is, however, a drawback in the excitation scheme which is the lack of selection on the sublevel m_J of the intermediate 5 D_J state populated in the dissociation process. This implies that several Rydberg series with $m=0$, 1, 2, or 3 can be excited according to the polarization. As L_z is a constant of motion in Stark effect, this indicates that the spectra reflect the independent superposition of several noninteracting series with different weights.

The electric field does not affect the fine structure ($\Delta E=97.588$ cm^{-1}) of the $5D$ states and the maximum Stark splitting of the sublevels is negligible ($\ll1$ GHz). The hyperfine structure is negligible. In the Rydberg spectra the hyperfine structure is negligible too. The fine structure of the $nP_{1/2}$, $nP_{3/2}$, $nD_{3/2}$, and $D_{5/2}$ states is

affected in the conventional way by the Stark effect. The fine structure can be considered negligible for the $nF, nG, \ldots$ series. The quantum defects of the states are $\delta(S)=4.06$, $\delta(P_{1/2})=3.592$, $\delta(P_{3/2})=3.559$, $\delta(D_{3/2})=2.475$, $\delta(D_{5/2})=2.466$, $\delta(F)=0.033$, $\delta(G)=0.007$. In zero field, the oscillator strength from the $5D$ to the nF series is 30 times that for those from $5D$ to nP.

Finally, σ polarization of the laser allows one to excite mainly $m=\pm 3$ Stark series, which involve states with $l \geq 3$ with negligible quantum defects. Hence the behavior will be nearly hydrogenic at the lowest field values.[11] In contrast π polarization of the laser leads to the excitation of $m=0, \pm 1, \pm 2$ series which involve nonhydrogenic S, P, or D states. This situation is basically nonhydrogenic and leads to Stark redistribution of nonhydrogenic states onto the incomplete manifold. In spite of the superposition of several series with different m, which are noninteracting, it is possible to experimentally discriminate between them.

C. Linear Stark effect on nonhydrogenic series

Several experimental examples have been shown previously for $m=\pm 3$ states[11,28] for which conditions are nearly the hydrogenic ones. That is, one observes the linear Stark quantization of a complete Stark manifold with $n-3$ components.

With π polarization of the laser, at low fields, one observes again a linear Stark spectrum (see Fig. 5). For $n=42$, it shows 39 components spaced with $2\omega_s$ and the spectrum can be shown to be nearly identical to the one for $|m|=3$. Actually, the spectrum reflects mainly the contribution from the $|m|=1$ states. This is the linear Stark spectrum of an incomplete manifold (see Sec. II D). The missing component is contained in the P and D states which are still energetically separated from the manifold.

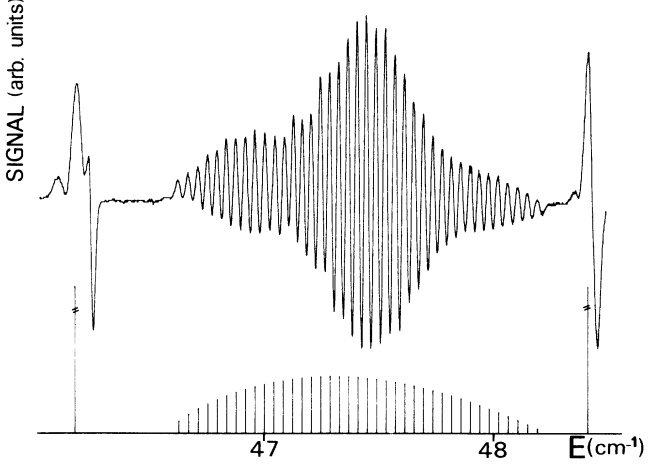

FIG. 5. Linear Stark effect on the ($n=42$, $m=1$) incomplete manifold of cesium at $F=7.30$ V/cm. The 39 components are spaced with $2\omega_s=1.18$ GHz (Doppler limited-frequency modulation of the laser). The P and D lines from nonhydrogenic states are seen on both sides. (Energy E in excess of 16 700 cm^{-1}.) The lower trace is the stick spectrum calculated from matrix diagonalization (see text, Sec. V).

D. Stark redistribution and generation of pseudo-Fano profiles

When the field is increased, the Stark redistribution of nonhydrogenic P and D states begins. This is shown in Fig. 6 for various field and n values, and, for reasons to be made clear below, this mainly concerns the series with $m=1$. As expected from Sec. III, the redistribution of the discrete states leads to the generation of pseudo-Fano profiles. According to the resolution $\Delta_D \simeq 1$ GHz compared to the spacing $\omega=2\omega_s$, the phenomenon appears continuous or discrete (see Fig. 2 of Ref. 12).

When the interaction begins, the redistribution is not complete. It affects the intensities and positions of about ten sublevels of the Stark manifold which indicates that the interaction occurs in the intermediate coupling case (Sec. III). Detailed interpretation of these patterns is given in Sec. V. Early experimental evidence for this effect exists in the plots in Ref. 1.

E. Stabilization of the quasibound Stark spectrum

From Fig. 6 it appears likely that an appropriate increase in the field value will allow the two profiles on each wing of the manifold to merge somewhere close to its center. What happens is shown on Fig. 7 for the $n=54$, $m=1$ Stark manifold. A sharp and intense line develops from the strongly competing channels at a well-defined field value. Its width is the Doppler width which indicates that it no longer interacts with the other Stark channels. This process is the "stabilization" of a discrete state in the quasi-continuum through interference effects.

This is in fact one of the most perfect experimental

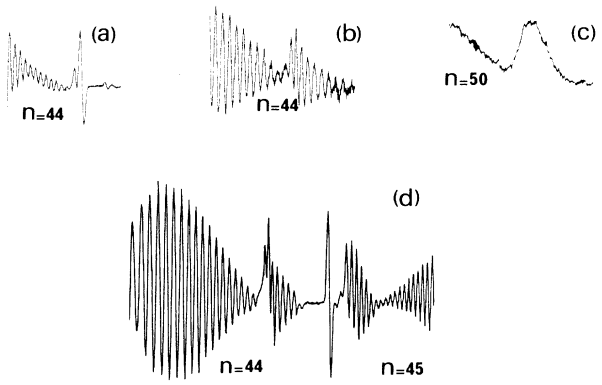

FIG. 6. Experimental examples of pseudo-Fano profiles seen in various conditions of n and F field values. According to the magnitude of the spacing $2\omega_s$ compared to the Doppler width (1 GHz), the phenomena may look continuous or not (Ref. 12). (a) $F=6.36$ V/cm (frequency modulation, FM); weak redistribution of the discrete state on the $n=44$ manifold. (b) $F=9.17$ V/cm (FM); intermediate redistribution regime. (c) $F=4.5$ V/cm (AM); same as (b), but the spacing is smaller than the Doppler width. The profile then looks continuous. (d) $F=8.40$ V/cm (FM); the redistribution on a larger scale showing the two states $|\varphi_{45}^{\pm}\rangle$ interacting with the $n=44$ and 45 manifolds (see Sec. V C).

realization of the situation considered in Sec. III D, where two discrete states are interacting with a quasicontinuum of discrete states. The full experimental story of the birth and death of the stabilized resonance is shown in Fig. 7 where it is demonstrated that the interference process is localized about a given field value. The amplitude-modulated plot (see Fig. 8) on a wider scale affords the evidence of the existence of another state, more strongly coupled to the manifold and leading to a large pseudo-Fano profile.

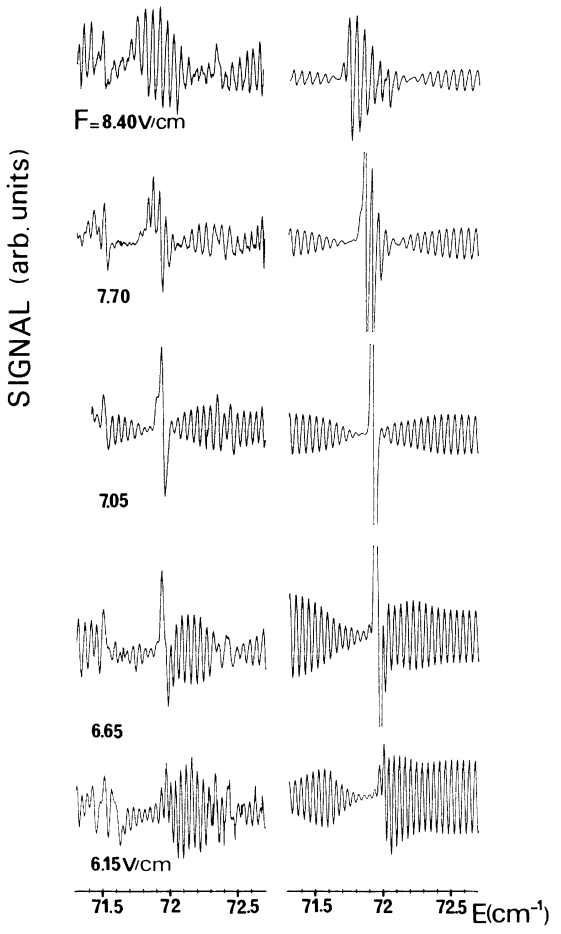

FIG. 7. Stabilization of a discrete state at the center of the $n=54$ manifold (frequency modulation spectroscopy; energy E in excess of 16 700 cm^{-1}). The local field-energy region is schematized on Fig. 4. The evolution of the phenomena can be observed for a large range of field values ($F=6.14$, 6.66, 7.04, 7.72, 8.42 V/cm from bottom to top) in the vicinity of a decoupling field amplitude which ranges between 7 and 7.25 V/cm (experimental spectra: left traces). The width of the line is then about 1 GHz (Doppler width). Comparison with the numerical theory at the same field values (right traces) shows satisfactory agreement with good reproduction of the main characters of the patterns, but not for the absolute values of the intensities (see text). The same phenomenon is shown at $F=7.25$ V/cm in the inset of Fig. 8, with amplitude modulation techniques. The broad modulation results from the other discrete state interfering with the manifold states which generates a Fano profile.

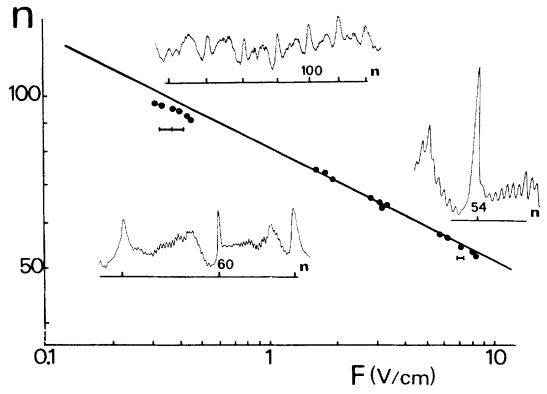

FIG. 8. Log-log plot of the decoupling field F_d for several n values between 50 and 100. The dotted line represents the theoretical prediction ($F_d n^5=0.67$, from Sec. V C). Experimental records with amplitude modulation techniques are shown in the insets exhibiting various stages of the stabilization process. (Field values: $F=0.35$ V/cm for $n=96$ to 102; $F=4.25$ V/cm for $n=59$ to 61; $F=7.25$ V/cm for $n=54$.)

This phenomenon obeys a $n^5F=$const scaling law (see Sec. V) and can be tracked from $n=40$ to $n=100$ in the Rydberg spectrum with the present range of field values. This is shown in Fig. 8.

V. DISCUSSION AND THEORETICAL INTERPRETATION

The model of Sec. III combined with proper evaluation of the nonhydrogenic matrix elements in cesium allows for a detailed interpretation of the experimental results. However, a detailed comparison of line intensities with theory requires a numerical approach. Diagonalization on 11 adjacents manifolds meets any stability requirements in the present range of field and n values.

In zero field, the nonhydrogenic P and D states lie out of the $m=1$ incomplete manifold (cf., Fig. 4). As the difference of their quantum defects $\delta(P)-\delta(D)$ is only 0.10 (mod. 1), that is far smaller than $|\delta(D)-\delta(F)|$ and $|\delta(P)-\delta(F)|$ (mod. 1), the two states $(n+3)P$ and $(n+2)D$ have nearly equal energies. At low field ($F\approx|\delta(P)-\delta(D)|n^{-5}$), they are mixed at first order by the Stark interaction while the mixing with the states of the incomplete manifold is negligible. The mixed components

$$|\varphi_n^{\pm}\rangle=\frac{1}{\sqrt{2}}(|n+2\ D\rangle\pm|n+3\ P\rangle) \tag{19}$$

exhibit a linear Stark effect. They constitute an effective two-level system weakly interacting with the $(n-3)$ levels of the n incomplete manifold.

At higher fields, the interaction of $|\varphi_n^{\mp}\rangle$ with the incomplete manifolds generates pseudo-Fano profiles. $|\varphi_n^{+}\rangle$ and $|\varphi_{n+1}^{-}\rangle$ are then the adiabatic states below and above the n manifold, respectively, that increase and decrease into the n manifold as F increases from zero. Fi-

nally, the energy curves associated with $|\varphi_n^+\rangle$ and $|\varphi_{n+1}^-\rangle$ (which are strongly mixed with the n manifold's parabolic channels) anticross. Near this point, a proper linear combination of the two states is stabilized with no interaction with the n manifold. This eigenstate is a superposition of low l states, with no contribution from the states of the incomplete n manifold.

A. Evaluation of the matrix elements

There are only eight matrix elements to evaluate as shown in Fig. 9. This is done using the method of Edmonds *et al.*[29,30] applied to situations where $l \ll n$

$$\langle n\, l\, m|z|n\, l+1\, m\rangle = \tfrac{3}{2}n^2\left[\frac{(l+1)^2-m^2}{(2l+1)(2l+3)}\right]^{1/2} \times g_0(\Delta n^*)\,, \tag{20}$$

where g_0 is tabulated in Ref. 29 with argument Δn^* the difference of the effective quantum numbers. The values of the matrix elements for cesium $m=1$ states are given in Table I.

B. Analysis of the experimental pseudo-Fano profiles

The energies of the discrete states $|\varphi_n^{\pm}\rangle$ [Eq. (19)] are $E_n^{\pm}=E_n^0\pm V_n$, where E_n^0 is the averaged energy of the $(n+3)P$ and $(n+2)D$ states and $V_n=d_1F=0.66n^2F$. The interaction of the $|\varphi_{n+1}^{\pm}\rangle$ states with, respectively, the $(n,m=1)$ and $(n+1,m=1)$ manifolds is through the $D\rightarrow F$ matrix element with $\langle\varphi_{n+1}^+|V|n+1F\rangle=d_3F/\sqrt{2}\simeq 0.40(n+1)^2F$ and $\langle\varphi_{n+1}^-|V|nF\rangle=d_5F/\sqrt{2}\simeq 0.35n^2F$. The distribution of the nF state onto the manifold can be evaluated assuming complete redistribution,[31] i.e., $\langle\psi_p|nF\rangle\propto n^{-1/2}$. Since the spacing is $\omega=2\omega_s$, this leads to $V_q^+/\omega\simeq 0.133\sqrt{n+1}$ and $V_q^-/\omega\sim 0.117\sqrt{n}$. From Eq. (14) the widths of the profiles are thus $\Gamma^+=0.33n^2F$ and $\Gamma^-=0.25n^2F$ (or $\Delta n^+=\Gamma^+/2\omega_s\simeq 0.11n$ and $\Delta n^-=0.08n$ spacings[31]).

Conditions for the generation of pseudo-Fano profiles are those described in Sec. IV where both the coupling and excitation of the channels are via the same $|nF\rangle$ component. From Eq. (17), Δ is given by $\Delta_n^+=d_3\xi^+/2=0.28n^2F\xi^+$ and $\Delta_n^-=-d_5\xi^-/2=-0.25n^2F\xi^-$ where $\xi^{\pm}$ stands for

$$\xi^+=\frac{\langle(n+4)P|T|5D\rangle}{\langle(n+1)F|T|5D\rangle}\,,\qquad \xi^-=\frac{\langle(n+4)P|T|5D\rangle}{\langle nF|T|5D\rangle}\,. \tag{21}$$

The modulus of $\xi^{\pm}$ is independent of n. The $\xi^{\pm}$ have opposite signs ($\xi^+=-\xi^-$). With the present phase conventions,[29] radial wave functions have the same signs at infinity. Hence $|nF\rangle$ and $|n+1\,F\rangle$ are in phase opposition close to the origin. Consequently, Δ_n^+ and Δ_n^- have same sign, equal to that of ξ^+ which is not known. The modulus of ξ^+ is $|\xi^+|=0.17$ from evaluations of the ratio of the matrix elements or measurements of the zero-field intensities of the P and F lines. Hence the shift Δ arising from the interference effect in optical excitation is of same sign, whatever the wing of the manifold and whatever the n value. From Sec. IV and Eq. (17), the profile is a minimum at $\varepsilon_q=-Q$ or $E-E_n^{\pm}=-\Delta_n^{\pm}$.

Finally, the shifts $F_q^{\pm}$ arising from the variations of the coupling are of opposite signs with the present distribution of the coupling (see Fig. 1). They shift the discrete states $|\varphi_n^{\pm}\rangle$ outwards. This implies that Fano parameters $Q^{\pm}$ are different [from Eq. (17)].

For the conditions of the plot in Fig. 10 the experimental values are $n=44$, $F=8.40$ V/cm, and $2\omega_s=1.4$ GHz. Fitting the two profiles, $|\varphi_{45}^-\rangle$ and $|\varphi_{45}^+\rangle$, leads to the experimental values $Q_{45}^-=2$, $\Gamma_{45}^-=3$ GHz, and $Q_{45}^+=-1.3$, $\Gamma_{45}^+=6$ GHz. The previous estimates leads to $\Gamma^-=2.8$ GHz and $\Gamma^+=3.6$ GHz. The underestimation of Γ^+ comes from the departure from equiredistribution of the $|45F\rangle$ state on the wing of the manifold (it is closer to $|\varphi_{45}^+\rangle$ due to the quantum defect $\delta=0.033$). Hence $(V_q^-)_{\text{theor}}\sim 0.8$ GHz, $(V_q^+)_{\text{theor}}\sim 0.9$ GHz while $(V_q^-)_{\text{expt}}\sim 0.8$ GHz and $(V_q^+)_{\text{expt}}\sim 1.16$ GHz.

Measurements of the position of the minimum of the profiles lead to $\Delta_{\text{expt}}^+=0.9$ GHz and $\Delta_{\text{expt}}^-=0.9$ GHz also (this is done by comparing to the positions $E_n^{\pm}$ of the discrete states $|\varphi_{45}^{\pm}\rangle$ evaluated from $\pm V_n$ or better by taking into account the interaction with the manifolds

TABLE I. Values of the nonhydrogenic matrix elements of the dipole (d_i) for the situation considered in Fig. 9. They are evaluated through Eq. (20) and Ref. 29 in atomic units for $m=1$ states. Notice that the phase convention here and in Ref. 29 is that radial wave functions are positive at infinity.

$d_1=\langle n+3\ P\|z\|n+2\ D\rangle$	$=0.66n^2$
$d_2=\langle n+3\ P\|z\|n+3\ D\rangle$	$=0.08n^2$
$d_3=\langle n+2\ D\|z\|n\ F\rangle$	$=0.56n^2$
$d_4=\langle n+2\ D\|z\|n+4\ P\rangle$	$=0.21n^2$
$d_5=\langle n\ F\|z\|n+3\ D\rangle$	$=0.50n^2$
$d_6=\langle n+4\ P\|z\|n+3\ D\rangle$	$\simeq d_1$
$d_7=\langle n+3\ D\|z\|n-1\ F\rangle$	$=-0.08n^2$
$d_8=\langle n+2\ D\|z\|n+1\ F\rangle$	$=-0.06n^2$
$d_9=\langle n-1\ F\|z\|n+2\ D\rangle$	$\simeq d_5$
$d_{10}=\langle n+3\ D\|z\|n+1\ F\rangle$	$\simeq d_3$

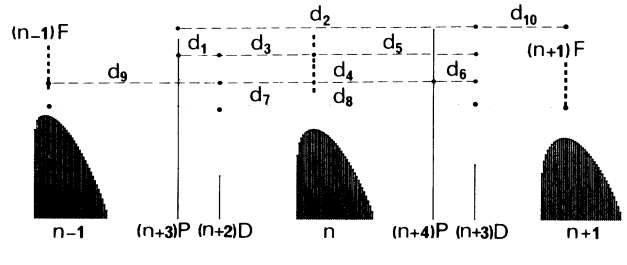

FIG. 9. Stark effect on $m=1$ states of cesium (theoretical simulation). The dipole matrix elements d_i can be evaluated simply from Ref. 29 and are sufficient for understanding the experimental results on Fano profiles and stabilization. Their numerical values are given in Table I.

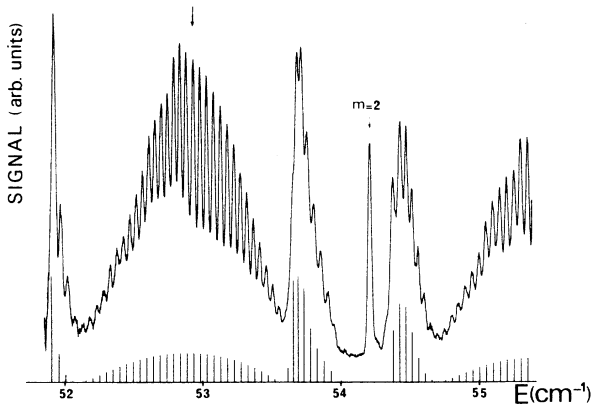

FIG. 10. Fano profile generation associated with the interaction of nonhydrogenic $m=1$ (P,D) states with the $n=44$ and 45 incomplete manifolds ($F=8.40$ V/cm; energy E in excess of 16 700 cm^{-1}; amplitude modulation). The difference in the appearance of the profiles (φ_{45}^{-}) and (φ_{45}^{+}) illustrates the main point in the theory of Fano profiles. The shift Δ due to the interference effect is towards high energy. The shift due to the variations of the coupling on the manifold is outwards. This leads to an enhancement of the asymmetry on the high-energy wing of the manifold and to a compensation on the low-energy wing. This general character of the patterns is stable whatever the n value. Comparison with numerical simulations (bottom trace) reveals excellent agreement for both the positions and shapes. However, the experimental intensities of the states of the manifold are too intense due to contributions from $m=2$ states. Actually, the $m=2$, $47D$ line is seen with high intensity, with a width comparable to the Doppler width. The arrow indicates the zero-field position of the $n=44$ hydrogenic manifold.

other than respectively $n=44$ or $n=45$). Hence the shift Δ is positive towards high energies and the sign of ξ^{+} is thus positive too. From these considerations, determination of the signs of the matrix elements in ξ^{+} can be obtained.

The determinations of $F_q^{\pm}$ are deduced from the values of Δ and Q. One obtains $(F_q^{-})_{\text{expt}}=1.5$ GHz and $(F_q^{+})_{\text{expt}}=-4.5$ GHz. Both shifts express a repulsion from the manifolds as expected. That they are very different comes from the slight asymmetry in the matrix elements, and especially from the fact that the $|45F\rangle$ is closer to $|\varphi_{45}^{+}\rangle$ leading to a departure from equipartition.

Finally, theoretical values from the full numerical calculations are $(F_q^{-})_{\text{theor}}=1.8$ GHz, $(\Gamma^{-})_{\text{theor}}=2.7$ GHz, $\Delta_{\text{theor}}^{-}=0.9$ GHz, and $(F_q^{+})_{\text{theor}}=-5$ GHz, $(\Gamma^{+})_{\text{theor}}=5.4$ GHz, $(\Delta^{+})_{\text{theor}}=0.9$ GHz, and thus compares fairly well with the experimental results.

All the major aspects of the theory of Fano profiles are thus illustrated here with simple calculations. The asymmetry of the profiles on the low and high energy wings of the manifold is mainly due to compensation on one wing and addition on the other, of the two Δ and F_q contributions to the Q parameter. This character holds true whatever the n value. Comparison with the numerical theory (Fig. 10) indicates a 100-MHz agreement so far as the position of the lines are concerned and fairly good reproduction of the shapes. But the experimental intensities of the manifold are enhanced by the superposition of contributions from $m=0$ and $m=2$ states due to the drawback in our excitation scheme (Sec. IV). From Sec. II D, we see that this adds an independent contribution with roughly the same spectrum, but does not add any new interference effects. As seen on the plot on Fig. 10 the $(m=2, 47D)$ line is still out of the manifold (its Stark effect in contrast with $m=1$ P and D states is quadratic[20]) and its width is still the Doppler width.

C. Analysis of the stabilization process

The interpretation of the experimental plots on Fig. 7 can be done in the same way. Comparison with numerical simulations reveal a fairly good agreement as concerns the positions of the lines and the position of the decoupling (in field and energy). Even far from decoupling, the shapes of the profiles agree. There is, however, a discrepancy in the intensities of the manifold lines which, as previously discussed, is due to contributions from essentially the $m=2$ series.

For $n=54$, the stabilization process involves $|\varphi_{55}^{-}\rangle$ and $|\varphi_{54}^{+}\rangle$ which interfere very close to the center of the $n=54$ manifold. The matrix elements involved in the theory of Sec. III D are (using the evaluations of Sec. V A and Table I): $\mathcal{V}_{11}\simeq 0.66(n-1)^2$ and $\mathcal{V}_{22}\simeq -0.66n^2$ and the coupling $\mathcal{V}_{12}$ between $|\varphi_{54}^{+}\rangle$ and $|\varphi_{55}^{-}\rangle$ is $\mathcal{V}_{12}=-0.07n^2$. Their coupling with the manifold is from Sec. V A $\mathcal{V}_1\simeq\mathcal{V}_2\simeq -0.37n^2F$. One deduces $F_d\sim 0.75/n^5$ and the energy $E_d\simeq -(1/2n^2)-(0.02/n^3)$. The decoupling takes place approximately at the zero-field energy of the n manifold which follows from the symmetrical character of the situation (the P and D states are nearly degenerate and at half distance from the manifolds). As $\mathcal{V}_{12}<0$, the decoupled state is

$$|\Phi_d\rangle=\frac{1}{\sqrt{2}}(|\varphi_{n+1}^{-}\rangle-|\varphi_n^{+}\rangle)$$
$$\simeq -\tfrac{1}{2}(|n+2\ D\rangle+|n+3\ P\rangle$$
$$-|n+3\ D\rangle+|n+4\ P\rangle)\,, \qquad (22)$$

while the other one leads to a large Fano profile (see Fig. 8 and Ref. 12) indicating a strong coupling with the Stark manifold. The decoupled state from Eqs. (19) and (22) is a superposition of four P and D states with low l values and is not mixed with the manifold's states.

However, this model is not completely satisfying as $|\Phi_d\rangle$ has a nearly zero probability of optical excitation. Actually $\langle\Phi_d|T|5D\rangle\sim\frac{1}{2}\{\langle n+4\ P|T|5D\rangle+\langle n+3\ P|T|5D\rangle\}\simeq 0$. The interference process is destructive which contradicts the experimental results. The origin lies in that the coupling of $|\varphi_{n+1}^{-}\rangle$ and $|\varphi_n^{+}\rangle$ with the $n+1$ and $n-1$ manifolds cannot be ignored as $\langle\varphi_{n+1}^{-}|V|n+1\ F\rangle\simeq 0.30/n^3$ at the decoupling, which is comparable to the distance of $|\varphi_{n+1}^{-}\rangle$ to the center of the $n+1$ manifold. Including these effects only weakly modifies the conclusions so far as the position is concerned due to the nearly symmetrical character of all ma-

trix elements. Using $\langle \varphi_n^{\pm} | V | n-1\ F \rangle \sim -0.36 n^2 F$, the field value at decoupling is

$$F_d = 0.67/n^5 \tag{23}$$

and the oscillator strength of the decoupled state is now $\langle \bar{\Phi}_d | T | 5D \rangle \sim -0.275 \langle nF | T | 5D \rangle$. The intensity of the decoupled line is thus about five times greater than those of the manifold for $n \simeq 50$.

Finally, the new field value of decoupling compares fairly well with experimental measurements between $n=50$ and 100, as shown in Fig. 8, and gives $(F_d)_{\text{expt}} = (0.67 \pm 0.04)/n^5$. That this value is twice the field value associated with crossing of the edge states of the n and $n \mp 1$ manifolds is an accident [it follows from the values of the matrix elements in Eq. (20)].

Further use of the model of Sec. III would allow detailed analytical studies of the width of the process against n and F as shown in Ref. 12.

VI. CONCLUSIONS

We have thus experimentally studied two basic phenomena of significant importance for the physics of the Stark effect on nonhydrogenic atoms. Studies have been done in the quasibound part of the spectrum which allows accurate measurements to be performed. The study of stabilization was here possible on a broad scale. Analytical interpretation of most of the features of the spectrum have been done with a model involving the interaction of one discrete state with a quasicontinuum of discrete states, which finds here one of its most perfect experimental realizations.

Both Fano-shaped profiles and stabilization effects are precursors of the processes previously seen in the continua region. The only difference is that the scattering width of the states is negligible in our conditions. States are quasibound states and not resonances, but, in both cases, the origin of phenomena is the same. It is the Stark redistribution of nonhydrogenic states onto the hydrogenic channels which results from the breaking of the Stark dynamical symmetry.

Such stabilized discrete states, having low angular momenta and being decoupled from the parabolic Stark channels at a nonzero electric field value may be of interest in the context of atoms manipulations with external fields[32] owing to their strong optical oscillator strengths allowing efficient laser excitation, as well as in collisional studies. Obviously, the tunability of the phenomena on the **F** field and on the n value is one more important character.

Very similar situations, involving quasicontinua of vibrational states are also expected to be found in molecules or other systems as Rydberg atoms in magnetic fields or crossed fields[33] and as well in autoionizing spectra.[34] This of course has great importance in the context of line-shape formation[35] and in analyzing the data in vapors or for plasmas diagnostics purposes.

ACKNOWLEDGMENTS

We would like to thank F. Biraben, F. Penent, W. Hartmann, and A. Steitz for their collaborations at various stages of the experimental work, and M. Glass-Maujean for extended discussions. The Laboratoire de Spectroscopie Hertzienne de l'Ecole Normale Supérieure is "Laboratoire associé au Centre National de la Recherche Scientifique (U.A.18)," à l'Ecole Normale Supérieure et à l'Université Paris VI.

---

*Present address: Laboratoire de Physique des Lasers, Université Paris-Nord, place J.B. Clément, 93430 Villetaneuse, France.

[1]M. L. Zimmerman, M. G. Littman, M. M. Kash, and D. Kleppner, Phys. Rev. A **20**, 2251 (1979).

[2]S. Feneuille, S. Liberman, J. Pinard, and A. Taleb, Phys. Rev. Lett. **42**, 1404 (1979).

[3]T. S. Luk, L. Di Mauro, T. Bergeman, and H. Metcalf, Phys. Rev. Lett. **47**, 83 (1981).

[4]D. A. Harmin, Phys. Rev. A **24**, 2491 (1981).

[5]D. A. Harmin, Phys. Rev. A **26**, 2656 (1982).

[6]D. A. Harmin, Phys. Rev. A **30**, 2413 (1984).

[7]E. Luc and A. Bachelier, J. Phys. B **13**, 1743 (1980); **13**, 1769 (1980).

[8]U. Fano, Nuovo Cimento **12**, 156 (1935).

[9]J. Y. Liu, P. McNicholl, D. Harmin, J. Ivri, T. Bergeman, and H. Metcalf, Phys. Rev. Lett. **55**, 189 (1985).

[10]C. Chardonnet, These, University Paris 6, Paris, 1983 (unpublished).

[11]C. Chardonnet, F. Penent, D. Delande, F. Biraben, and J.-C. Gay, J. Phys. Lett. **44**, L517 (1983).

[12]C. Chardonnet, D. Delande, and J.-C. Gay, Opt. Commun. **51**, 249 (1984).

[13]P. J. Redmonds, Phys. Rev. A **133**, 1352 (1964).

[14]P. F. O'Mahony and K. T. Taylor, Phys. Rev. Lett. **57**, 2931 (1986).

[15]S. Feneuille, S. Liberman, E. Luc-Koenig, J. Pinard, and A. Taleb, J. Phys. B **15**, 1205 (1982).

[16]W. van de Vater, D. R. Mariani, and P. M. Koch, Phys. Rev. A **30**, 2399 (1984).

[17]S. P. Alliluyev and I. A. Malkin, Zh. Eksp. Teor. Fiz. **66**, 1283 (1974) [Sov. Phys.—JETP **39**, 627 (1974)].

[18]H. J. Silverstone and P. M. Koch, J. Phys. B **12**, L537 (1978).

[19]R. J. Damburg and V. V. Kolosov, J. Phys. B **12**, 2637 (1979).

[20]F. Penent, C. Chardonnet, D. Delande, F. Biraben, and J.-C. Gay, J. Phys. (Paris) **44**, C7, 193 (1983).

[21]F. Penent, D. Delande, and J.-C. Gay, Phys. Rev. A **37**, 4707 (1988).

[22]C. Fabre, Y. Kaluzny, R. Calabrese, Liang Jun, P. Goy, and S. Haroche, J. Phys. B **17**, 3217 (1984).

[23]U. Fano, Phys. Rev. A **124**, 1866 (1961).

[24]C. Cohen-Tannoudji and P. Avan, in *Colloque International C.N.R.S. no. 273, Aussois, France, 1977*, edited by S. Feneuille and J. C. Lehman, (Les Editions du CNRS, Paris, 1977).

[25]According to our definition of $\{E'_q; 1 \le q \le N+1\}$ and $\{|\chi_q\rangle\}$, $|\psi_q\rangle$ is the state of the unperturbed manifold which energy E_q is just above E'_q. In Eqs. (7)–(11) and (13)–(16), choosing $|\psi_{q-1}\rangle$ instead of $|\psi_q\rangle$ (with $E_{q-1} < E'_q < E_q$) would not alter

the physical conclusions, provided the variations of V_q and T_q are smooth.

[26]Numerous examples are discussed in *Abstracts of Invited Lectures of C.N.R.S.—Round Table, Gif/Yvette, 1987,* edited by M. Aymar and A. Giusti (Université Paris–Sud, Orsay, 1987).

[27]J.-C. Gay, D. Delande, and F. Biraben, J. Phys. B **13**, L729 (1980).

[28]F. Penent, D. Delande, F. Biraben, C. Chardonnet, and J.-C. Gay, in *Laser Spectroscopy VI,* edited by H. P. Weber and W. Lutty (Springer, New York, 1983).

[29]A. R. Edmonds, J. Picart, N. Tran Minh, and R. Pullen, J. Phys. B **12**, 2781 (1979).

[30]D. Delande, Thése de Doctorat d'Etat ès Sciences, Université Paris 6, Paris, 1988 (unpublished).

[31]The hypothesis of complete redistribution implies that Δn and V_q/ω do not depend on the F field. This is likely to be roughly correct in the wings and at low fields only. This also can be evaluated using the general method in Ref. 6.

[32]D. Delande and J.-C. Gay, Europhys. Lett. **5**, 303 (1988).

[33]H. Rinneberg *et al.*, Phys. Rev. Lett. **55**, 382 (1985).

[34]J. Neukammer, H. Rinneberg, G. Jonsson, W. E. Cooke, H. Hieronimus, A. Koenig, K. Wietzke, and H. Spinger-Bolk, Phys. Rev. Lett. **55**, 1979 (1985).

[35]P. McNicholl, T. Bergeman, and H. Metcalf, in *Proceedings of the 8th International Conference on Spectral Lineshapes, Williamsburg, VA, 1986,* edited by R. J. Exton (Deepak, Hampton, 1987); P. McNicholl, T. Bergeman, and H. Metcalf, Phys. Rev. A **37**, 3302 (1988).